Kinetics of $NCl(a^1\Delta)$ via Photodissociation of ClN_3

Thomas L. Henshaw,* Samuel D. Herrera, Gregory W. Haggquist,† and L. A. (Vern) Schlie

Laser and Imaging Directorate, Phillips Laboratory (PL/LIDD), 3550 Aberdeen Ave., SE, Kirtland AFB, New Mexico 87117

Received: September 4, 1996; In Final Form: March 24, 1997[⊗]

Kinetic measurements of $NCl(a^1\Delta)$ metastables produced by the photolysis of chlorine azide (ClN_3) at 193 nm are reported. High $NCl(a^1\Delta)$ density ($>10^{15}$ molecules/cm^3) production facilitates measurements of the $NCl(a^1\Delta) + NCl(a^1\Delta)$ self-annihilation rate. A gas phase transient chemical titration scheme is used to calibrate absolute $NCl(a^1\Delta)$ density. The $NCl(a^1\Delta)$ bimolecular rate coefficient at room temperature is $(7.2 \pm 0.9) \times 10^{-12}$ cm^3/(molecule s) and has a magnitude very critical to the development of an $NCl(a^1\Delta) + I(^2P_{3/2}) \rightarrow I^*(^2P_{1/2}) + NCl(X^3\Sigma^-)$ chemical laser. Despite the large value of the self-annihilation rate, intense $I^*(^2P_{1/2})$ emission via transfer from $NCl(a^1\Delta)$ is strongly observed when mixtures of CH_2I_2 and ClN_3 are photolyzed at 193 nm. Unlike the analogous $O_2(a^1\Delta) + I(^2P_{3/2})$ energy transfer system, the relatively large $NCl(a^1\Delta)$ bimolecular rate constant suggests that $NCl(a^1\Delta)$ transport times must be short and will require small chemical mixing regions for efficient lasing. In addition, the 300 K collisional quenching rate constants of $NCl(a^1\Delta)$ by F_2, Cl_2, and Br_2 are $(2.5 \pm 1.1) \times 10^{-13}$, $(2.9 \pm 0.6) \times 10^{-11}$, and $(1.4 \pm 0.2) \times 10^{-10}$ cm^3/(molecule s), respectively.

Introduction

Metastable atoms and diatomic molecules have long been recognized for their importance as intermediates in atmospheric and combustion chemistry and in plasma and laser media. For example, in the near-infrared COIL chemical laser system[1,2] the $O_2(a^1\Delta)$ metastable pumps the $I^*(^2P_{1/2}) \rightarrow I(^2P_{3/2})$ lasing transition at 1.315 μm through the resonant energy transfer reaction between $O_2(a^1\Delta)$ and ground state $I(^2P_{3/2})$. In this vein, a considerable amount of attention has been given to the isovalent $NF(a^1\Delta)$ and $NCl(a^1\Delta)$ metastables as energy carriers in chemical lasers.[3,4] Of these, the $NCl(a^1\Delta)$ metastable appears particularly viable as an energy carrier in a chemically pumped system since $NCl(a^1\Delta)$ efficiently pumps $I^*(^2P_{1/2})$ via collisions with ground state $I(^2P_{3/2})$ in a flow system,[5,6]

$$Cl + N_3 \rightarrow NCl(a^1\Delta) + N_2 \qquad (1)$$

$$NCl(a^1\Delta) + I(^2P_{3/2}) \rightarrow NCl(X^3\Sigma^-) + I^*(^2P_{1/2}) \qquad (2)$$

generating a population inversion between the $I(^2P_{1/2}-{}^2P_{3/2})$ hyperfine states.[7] Recently, an $NCl(a^1\Delta)$ to $I(^2P_{3/2})$ energy transfer laser was demonstrated from the photolysis of chlorine azide (ClN_3) and CH_2I_2 gas mixtures at 193 nm.[8]

For $NCl(a^1\Delta)$ to be practical as an energy source in chemical lasers, several issues need to be understood. These include the generation of high $NCl(a^1\Delta)$ densities, determination of absolute $NCl(a^1\Delta)$ concentration, identification of $NCl(a^1\Delta)$ quenching species and their temperature-dependent rate constants, total rate constant and branching fraction, and the transfer rates to the laser candidate species. In the COIL system, the principal transport issues for singlet oxygen are the $O_2(a^1\Delta)$ energy pooling rate to produce $O_2(b^1\Sigma)$ and second-order removal rates such as the $O_2(a^1\Delta)-O_2(a^1\Delta)$ self-annihilation rate. Since these rates are small,[9] the transport of high concentrations of $O_2(a^1\Delta)$ to the iodine mixing nozzle occurs over large distances enabling high COIL powers of greater than 1 kW as reported by Fujii et al.[10] Similarly, for a successful scale-up of an $NCl(a^1\Delta)$-based laser system, a critical evaluation of $NCl(a^1\Delta)$ second-order self-removal rate must also be determined. In this paper, we report on the development of a gas phase titration scheme to measure the absolute $NCl(a^1\Delta)$ densities obtained from the photodissociation of ClN_3. Rate constant measurements for the bimolecular self-removal rate constant of $NCl(a^1\Delta)$ at high densities and other species are made. The magnitude of the bimolecular rate constant and its implications for an $NCl(a^1\Delta)-I^*(^2P_{1/2})$ chemical laser are discussed.

Experimental Section

The experimental apparatus is divided into three sections: a ClN_3 generator, an optical diagnostic on the ClN_3 generator flow, and a laser photolysis cell for $NCl(a^1\Delta)$ production.

ClN_3 Generator. Access to a large $NCl(a^1\Delta)$ density regime ($>10^{15}$ molecules/cm^3) is critical in understanding the bimolecular self-annihilation rate coefficient of $NCl(a^1\Delta)$. High densities are produced by the pulsed ArF photolysis of flowing chlorine azide mixtures at 193 nm. The most widely used method for synthesizing chlorine azide is the reaction of chlorine gas with water-moistened sodium azide (NaN_3) deposited on a glass wool support.[11] Since the duration of these experiments extended well beyond the conventional reactor lifetime of 1−2 h, a modification to the reactor design was made. The new ClN_3 generator is depicted in Figure 1. The generator is comprised of two parts: a Pyrex reactor (40 cm × 5 cm o.d.) where Cl_2 and water-moistened NaN_3 react to form chlorine azide and a dryer (30 cm × 5 cm o.d.) filled with anhydrous calcium sulfate to remove water vapor from the ClN_3 stream. Both the reactor and dryer are jacketed with recirculating water cooled to 5 °C. The principal modification to the synthesis is the use of a Pyrex tube, 25 cm long × 3 cm in diameter, where upon NaN_3 and Cl_2 react to form ClN_3. The reactor is prepared by laying flat a 1 cm thick × 15 cm wide × 25 cm long blanket of glass wool and evenly distributing 10−15 g of sodium azide (Kodak, 99.9%) onto the wool and subsequently wetting with 5 mL of deionized water (10 MΩ resistance). The wool is then wrapped around the Pyrex tube, moistened with 2 mL of water,

† Currently at TPL Inc., Albuquerque, NM 87120.

⊗ Abstract published in *Advance ACS Abstracts,* May 1, 1997.

S1089-5639(96)02745-4 CCC: $14.00

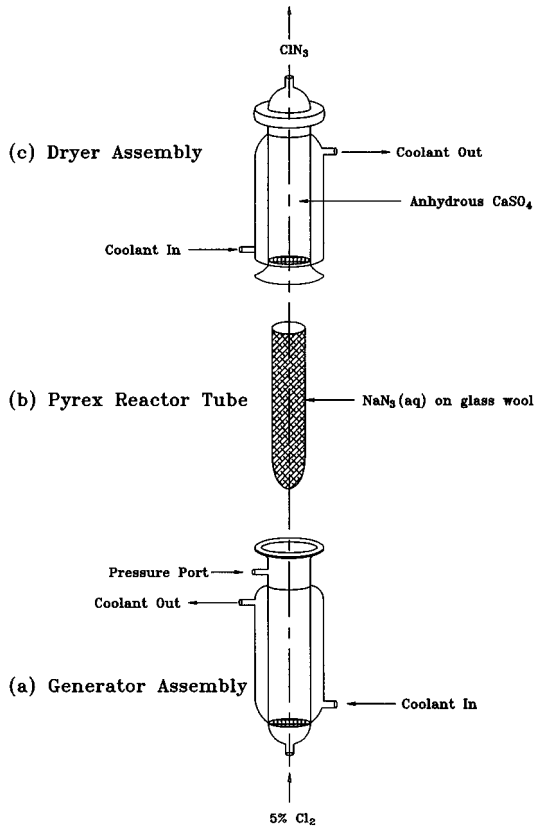

Figure 1. Diagram of the ClN_3 generator. (a) Generator housing with Cl_2 entrance, reactor pressure, and coolant input/output ports. (b) Insertable reaction tube where moistened NaN_3 on glass wool is wrapped around the tube and the $Cl_2 + NaN_3$ reaction occurs. (c) Reactor dryer housing with ClN_3 exit and coolant input/output ports. The last chamber is filled with anhydrous calcium sulfate to remove H_2O from the flow.

sprinkled again with 10 g of sodium azide, and then inserted into the reactor. In this manner, we are able to generate a stable ClN_3 flow for several hours per day for a period of a week or longer.

Photolysis Cell. Initial NCl($a^1\Delta$) transient emission results were obtained using a simple 5 × 3 cm aluminum cell fitted with UV grade fused silica windows and a liquid N_2 cooled intrinsic germanium detector (ADC, Inc., Model 403HS). However, this design proved unreliable for several reasons. First, considerable background window fluorescence and/or scattered light was found to be coincident with the NCl($a^1\Delta$) emission at 1.08 μm produced via 193 and 248 nm photolysis despite the use of an interference filter. Furthermore, the background emission was similar in magnitude and decay time to the NCl($a^1\Delta$) fluorescence and could not be separated from the NCl($a^1\Delta$) decay. Finally, the time constant for an intrinsic Ge detector is approximately 15 μs, and a significant portion of the early NCl($a^1\Delta$) time decay is lost due to the slow time response of this Ge detector. To eliminate the background fluorescence from the NCl($a^1\Delta$) emission, a new photolysis cell was fabricated and is shown in Figure 2. The photolysis cell consists of a 20 cm × 2.5 cm i.d. aluminum tube. The ClN_3 reactor flow and quenching gases were injected into the cell through a 90 cm × 2.5 cm i.d. Pyrex side arm. The background fluorescence was further minimized by anodizing the cell black, inserting light baffles along the laser axis, and using laser entrance and exit Brewster windows. Enhanced NCl($a^1\Delta$) transient response time was obtained using a S1 photomultiplier (Hamamatsu R1767, 8% quantum efficiency at 1.06 μm) cooled to −70 °C. The excimer laser (Questek Series 2000) was operated at the ArF and KrF wavelengths with a repetition rate of 0.5−1.0 Hz to allow the replacement of reagent gases before each laser pulse. The beams were focused into the aluminum cell, producing laser fluences of 70−200 mJ/cm^2. The excimer laser energy was measured by a Scientech (Model PHD 50) energy meter. All emissions were observed 90° to the incident laser beam. The NCl($a^1\Delta$) fluorescence was isolated with a 1.075 μm interference filter (0.01 μm bandwidth) and recorded with a 500 MHz digital oscilloscope (Tektonix TDS 544A). Spectral scans of the near-IR emission produced by ClN_3 photolysis were recorded with a 0.3 m monochromator having a 1 μm blazed grating (300 grooves/mm) coupled to a liquid nitrogen cooled intrinsic germanium detector (ADC Model 403LS) and processed by an SRS Model 250 boxcar averager. The fluorine and chlorine gas mixtures used in the titration and quenching experiments were 5% in helium (Matheson) and 20% in argon (Matheson), respectively. Gas mixtures of bromine (5% in helium) for the titration and quenching experiments were prepared by evaporation of liquid Br_2 (Aldrich, 99%) into a Pyrex storage vessel and diluting the vapor in helium (Matheson, UHP). The bromine was purified by a freeze−pump−thaw cycle before using. Similarly, a 0.5% mixture of CH_2I_2 (Fluka, >98%) in helium was prepared for the NCl($a^1\Delta$)−I($^2P_{3/2}$) energy transfer demonstration. Gas flow measurements were made with calibrated mass flow controllers (MKS Model 2258) while pressures were measured with a capacitance manometer (MKS Baratron Model 127A).

Optical Diagnostics. Due to a limitation in reactor conversion efficiency, a finite amount of Cl_2 is entrained in the ClN_3 flow. The rate constant for quenching[12] of NCl($a^1\Delta$) by Cl_2 is $(1.8 \pm 0.3) \times 10^{-11}$ cm^3/(molecule s) and thus, significant quenching of NCl($a^1\Delta$) by background Cl_2 is possible. Hence, the photolysis cell included a dual beam arrangement (90 cm path length) for *in situ* background Cl_2 density measurements and is shown in Figure 2. A HeCd laser (Omnichrome Series 56, 1 mW power) operated at 325 nm provided the sample and reference beams. The beams are sent to a 0.3 m monochromator equipped with a photomultiplier tube (RCA C31034) and a lock-in amplifier (Stanford Research Systems, Model 5029) for detection. The detector response was linear as determined by the transmission properties of several neutral density filters. Chlorine absorption measurements made on the ClN_3 stream revealed variable Cl_2 concentrations ranging from 0 to 30% of the total ClN_3 density and were found to be a function of the ambient factors controlling the synthesis. These include the chlorine flow rate and passivation of the reactor and ClN_3 transport surfaces. At high Cl_2 flow rates (greater than 50 sccm), the chlorine residence time in the reactor is too short for quantitative conversion to ClN_3, and thus the optimal reactor flow and pressure conditions for the ClN_3 synthesis were a 20 sccm flow of a 5% Cl_2 mixture in argon (Matheson) at a total pressure of 80 Torr. Furthermore, after several days of reactor conditioning the ClN_3 efficiency improved to near unity as no Cl_2 was detected in the reactor effluent. Because of the high conversion efficiency of ClN_3 here, it was deemed useful to record the UV absorption spectrum for calculating *in situ* ClN_3 densities and the corresponding fractional dissociation of ClN_3 from the laser pulse. The UV absorbance spectrum of ClN_3 was obtained with a Cary 5E spectrometer. In calculating the UV absorption cross sections, it is assumed that the Cl_2 is fully converted into ClN_3 such that the ClN_3 density is 5% of the total reactor effluent. This assumption is verified by the lack of Cl_2 detected in the effluent as evident from the absorption at 325 nm. Figure 3 shows the ClN_3 absorption spectrum in the region from 180 to 300 nm at a total pressure of 44.5 Torr and

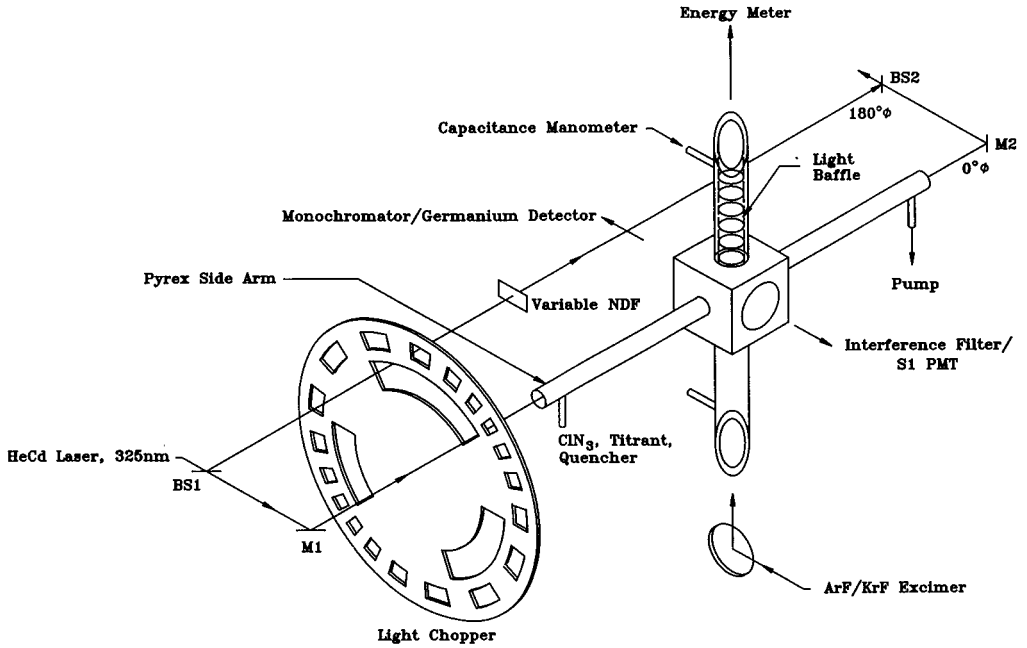

Figure 2. Diagram of the laser photolysis cell/titration apparatus. BS1 and BS2 are beam splitters, M1 and M2 are mirrors, NDF is a neutral density filter, and ϕ is the phase angle of the sample and reference beams.

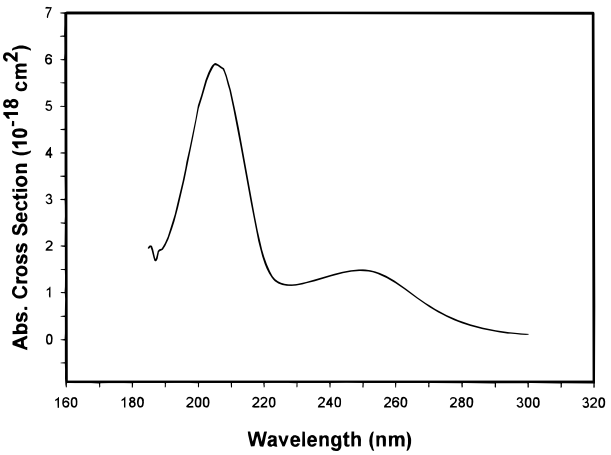

Figure 3. Ultraviolet absorption spectrum of ClN_3 (path length 15 cm, 5% ClN_3 in Ar, total pressure 44.5 Torr).

a path length of 15 cm. The spectrum gives an absorption cross section of 2.6×10^{-18} cm^2 at 193 nm and 1.5×10^{-18} cm^2 at 248 nm. An on-line FTIR spectrometer (MIDAC, Model M1210, 2 cm^{-1} resolution) continuously monitored the ClN_3 density prior to its injection into the photolysis cell using the asymmetric stretch of N_3 at 2060 cm^{-1}. Quantitative ClN_3 measurements in the IR were obtained by calibrating the N_3 asymmetric absorbance to the UV absorption at 250 nm. Figure 3 reveals a value of 1.5×10^{-18} cm^2 at 250 nm and is used to infer an IR absorption cross section of 4.9×10^{-19} cm^2 at 2060 cm^{-1}. Typical photolysis cell densities were 1×10^{16} molecules/cm^3 of ClN_3 mixed with an Ar carrier gas density of 2.2×10^{17} atoms/cm^3.

Results and Discussion

ClN_3 Photolysis. For the laser fluences available a substantial amount of undissociated ClN_3 is calculated to exist in the photolysis volume.[13] For example, up to 75% of the initial ClN_3 remains after photolyzing the sample with a laser fluence of 134 mJ/cm^2. In addition, the 193 and 248 nm photolysis of ClN_3 liberates more energy than is required for NCl($a^1\Delta$) production.[14] It has been postulated this excess energy produces vibrationally excited $N_2(X,v)$.[12] Since the KrF/ArF photolysis of ClN_3 produces NCl($a^1\Delta$) via the chain reaction of $N_2(X,v)$ with undissociated ClN_3,[8,12] it was necessary to examine the effect of secondary chemical processes within the photolysis medium. Figure 4 shows a comparison of the NCl($a^1\Delta-X^3\Sigma^-)_{v=0}$ time decay resulting from the 193 and 248 nm photolysis of ClN_3. The 248 nm induced photolysis exhibits a slow NCl($a^1\Delta$) time decay lasting for many milliseconds. In the context of the chain decomposition of ClN_3, the long decay here is suggestive of the removal of ClN_3 by $N_2(X,v)$ and the subsequent regeneration of NCl($a^1\Delta$). In contrast, the 193 nm photolysis produces a relatively rapid time decay of several hundred microseconds. To determine the magnitude of the NCl($a^1\Delta$) chain formation at 193 nm, experiments were conducted by varying the laser intensity and initial ClN_3 density and observing the tail of the NCl($a^1\Delta$) decay profile. In particular, the effect of changing the ArF intensity on the time decay of NCl($a^1\Delta$) at two widely different laser fluences of 143 and 14 mJ/cm^2 was studied. At the higher fluence, more $N_2(X,v)$ should be formed and a significant enhancement in the intensity of the NCl($a^1\Delta$) tail region should be seen. However, we observed for the high-fluence case no appreciable enhancement in the intensity of the tail relative to the low-fluence case, thus suggesting the chain chemistry is minimal under these conditions. Similar results were obtained for different ClN_3 densities at constant fluence. Thus, to simplify the kinetic analysis here the 193 nm photolysis wavelength is utilized.

NCl($a^1\Delta$) Bimolecular Self-Annihilation Rate. The decay of NCl($a^1\Delta$) is initially treated using the following kinetic scheme:

$$\mathrm{NCl}(a^1\Delta) \rightarrow \mathrm{NCl}(X^3\Sigma^-) + h\nu\ (1.08\ \mu\mathrm{m}) \quad (3)$$

$$\mathrm{NCl}(a^1\Delta) + \mathrm{NCl}(a^1\Delta) \rightarrow \text{products} \quad (4)$$

$$\mathrm{NCl}(a^1\Delta) + ClN_3 \rightarrow \text{products} \quad (5)$$

$$\mathrm{NCl}(a^1\Delta) + Cl_2 \rightarrow \text{products} \quad (6)$$

$$\mathrm{NCl}(a^1\Delta) + \mathrm{Ar} \rightarrow \mathrm{NCl}(X^3\Sigma^-) + \mathrm{Ar} \quad (7)$$

Reaction 3 is the radiative decay of NCl($a^1\Delta$) to its electronic ground state, $k_r \approx 0.7$ s^{-1}, and is negligible compared to other

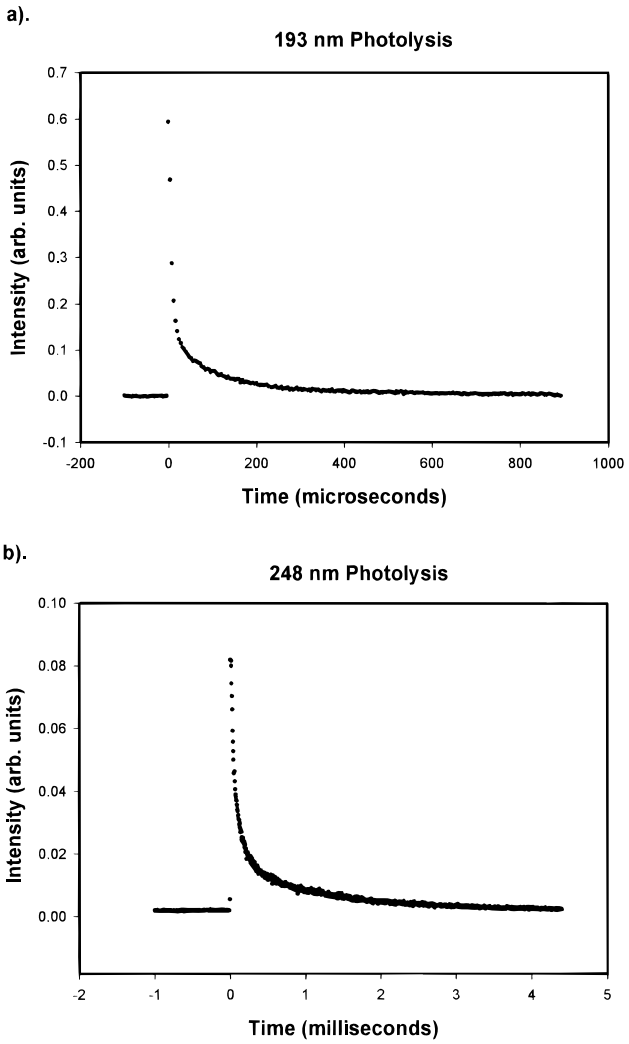

Figure 4. Time profile of the NCl(a−X)$_{v=0}$ emission produced by 193 nm photolysis of ClN_3. Photolysis conditions: laser fluence = 67 mJ/cm^2, ClN_3 density = 7.4×10^{15} molecules/cm^3, total pressure= 4.6 Torr. (b) Time profile of the NCl(a−X)$_{v=0}$ emission produced by 248 nm photolysis of ClN_3. Photolysis conditions: laser fluence = 280 mJ/cm^2, ClN_3 density = 6.0×10^{15} molecules/cm^3, total pressure = 5.2 Torr.

removal rates in this system.[15] The bimolecular reactions 4 and 5 represent the NCl($a^1\Delta$) self-removal and residual ClN_3 quenching. The absorption measurements of Cl_2 for the conditions described in Figure 4a indicate the chlorine concentration is small (less than 10% of the ClN_3), and process 6 can be ignored. Similarly, the quenching by the reactor carrier gas Ar is slow, $k \leq 10^{-15}$ cm^3/(molecules s), and process 7 can be disregarded.[12] Lateral diffusion may also affect the observed decay of NCl(a), but at total pressures above 2 Torr the diffusional losses become small.[12] Thus, the loss of NCl($a^1\Delta$) is reduced to a system of concurrent second-order and mixed second-order decays described by reactions 4 and 5:

$$\frac{-\mathrm{d}[\mathrm{NCl}(a^1\Delta)]}{\mathrm{d}t} = k_2[\mathrm{NCl}(a^1\Delta)]^2 + k'_2[\mathrm{NCl}(a^1\Delta)][ClN_3] \quad (8)$$

where k_2 is the second-order rate coefficient for the self-annihilation of NCl($a^1\Delta$) and k'_2 is the removal of NCl($a^1\Delta$) by collisions with undissociated ClN_3. In this model, the quenching of NCl($a^1\Delta$) by residual ClN_3 is treated as a physical process, NCl($a^1\Delta$) + $ClN_3 \rightarrow$ NCl($X^3\Sigma^-$) + ClN_3, where the amount of residual ClN_3 remains constant with respect to NCl($a^1\Delta$). Thus, the product of k'_2 and ClN_3 is combined into a single rate

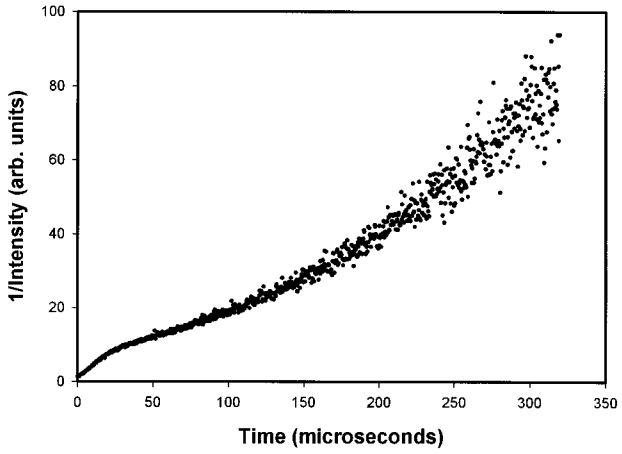

Figure 5. Plot of 1/NCl(a) intensity vs time illustrating a complex NCl(a) decay profile.

constant, k'_1, and the integrated solution of reaction 8 follows:

$$I(t) = \frac{k'_1[\mathrm{NCl}(a)]_0}{\exp(k'_1 t)(k_2[\mathrm{NCl}(a)]_0 + k'_1) - k_2[\mathrm{NCl}(a)]_0} \quad (9)$$

where $I(t)$ is the observed NCl($a^1\Delta$) intensity at time t and [NCl(a)]$_0$ the initial intensity of NCl($a^1\Delta$) at $t = 0$.

Because of the presence of a mixed second-order component, a simple second-order treatment to obtain the bimolecular self-annihilation rate constant is precluded. Indeed, Figure 5 displays a second-order plot of 1/ NCl($a^1\Delta$) intensity vs time and clearly shows the presence of a complex decay. To determine the bimolecular rate constants k_2 and k'_2, the NCl($a^1\Delta$) intensity must be calibrated to absolute number densities. A gas phase titration of NCl($a^1\Delta$) by Br_2 was used to measure absolute densities and is discussed in detail in the Appendix. This method involves quenching the NCl($a^1\Delta$) fluorescence to zero intensity with known amounts of an added quencher. At zero intensity lies the end point where the amount of added quencher equals the initial NCl($a^1\Delta$) density. An NCl($a^1\Delta$) titration by Br_2 is presented in Figure 11. The titration is collected under the photolysis conditions described in Figure 4a. A least-squares fit to the linear portion of the plot and extrapolation to the Br_2 axis gives an intersecting end point of (2.4 ± 0.2) $(2\sigma) \times 10^{15}$ molecules/cm^3 where the uncertainty represents the accumulation of error from the least-squares fit and determining the titrant number density from mass flow calculations. Several NCl($a^1\Delta$) titrations were performed at various ClN_3 densities and are summarized in Table 1. Using these titration data, an overall conversion efficiency (ϵ) of NCl($a^1\Delta$) density produced per ClN_3 dissociated can be calculated from the following: ϵ = NCl($a^1\Delta$)$_0$/([ClN_3]$_i$ − [ClN_3]$_0$), where NCl($a^1\Delta$)$_0$ is the initial density from the titration, [ClN_3]$_i$ is the initial starting ClN_3 density before the laser pulse, and [ClN_3]$_0$ is the residual ClN_3 density after the laser pulse. Accordingly, an average NCl($a^1\Delta$) yield of 60 ± 18% is obtained.

The extraction of the second-order rate constants is obtained through a nonlinear least-squares fit of eq 9 to the observed decay profile in Figure 4a. The error analysis in Figure 6 clearly shows the data are not well described by the concurrent second-order decays of reactions 4 and 5, indicating a significant decay contribution from an unknown source. The NCl($a^1\Delta$) emission in Figure 4a is comprised of two distinct decay components: a fast decay of several tens of microseconds followed by a slower decay of several hundred microseconds. A complex decay as shown here sometimes signifies the presence of a multicomponent decay attributed to several simultaneous and independent

TABLE 1: Summary of Titration Data and Second-Order Rate Constants

titration	initial ClN_3 (molecules/cm^{-3})	titrated NCl($a^1\Delta$) (molecules/cm^{-3})	k_2 (NCl($a^1\Delta$)) (cm^3/molecule s)	k'_2 (ClN_3) (cm^3/molecule s)
1	1.2×10^{16}	$(2.8 \pm 0.2) \times 10^{15}$	$(7.2 \pm 0.9) \times 10^{-12}$	$(6.8 \pm 1.7) \times 10^{-13}$
2	7.1×10^{15}	$(2.2 \pm 0.6) \times 10^{15}$	$(6.1 \pm 0.8) \times 10^{-12}$	$(7.6 \pm 1.9) \times 10^{-13}$
3	7.4×10^{15}	$(2.4 \pm 0.6) \times 10^{15}$	$(7.5 \pm 0.9) \times 10^{-12}$	$(5.7 \pm 1.4) \times 10^{-13}$
4	4.9×10^{15}	$(2.3 \pm 0.3) \times 10^{15}$	$(8.0 \pm 1.0) \times 10^{-11}$	$(1.4 \pm 0.4) \times 10^{-12}$
5	2.0×10^{15}	$(8.2 \pm 2) \times 10^{14}$	$(7.0 \pm 0.9) \times 10^{-12}$	$(2.7 \pm 0.7) \times 10^{-13}$
			av $(7.2 \pm 0.9) \times 10^{-12}$	av $(7.4 \pm 4.7) \times 10^{-13}$

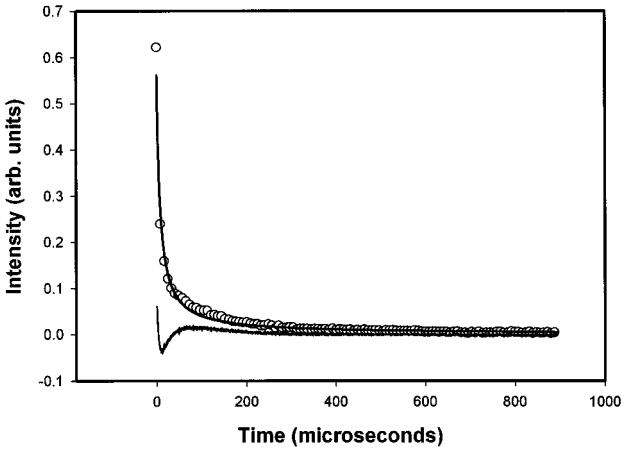

Figure 6. Nonlinear least-squares fit (solid line) of the model described by eq 9 to the observed NCl(a) decay (○) in Figure 4a. The lower trace is the residual analysis of the least-squares fit.

processes. Since the photolysis of ClN_3 at 193 nm produces nitrogen metastables and is exothermic enough to produce $N_2(B^3\Pi_g)$ directly,[11] a spectral scan of the near-IR emission was performed. The presence of nitrogen metastables was confirmed by the observation of the (0,0) band of the first positive $N_2(B^3\Pi_g - A^3\Sigma^+_u)$ system near 1.04 μm. To check for $N_2(B^3\Pi_g)$ emission in the vicinity of NCl($a^1\Delta$), a spectrum in the wavelength region from 1.06 to 1.095 μm was measured as shown in Figure 7. The spectrum was recorded with a ClN_3 density of 5×10^{15} molecules/cm^3 at a 1 μs delay with a gate width of 1 μs on the boxcar integrator. The spectral bandwidth of the monochromator was 2 nm. The presence of the (1,1) band of NCl($a^1\Delta$) at 1.069 μm suggests that NCl($a^1\Delta$) is produced with vibrational excitation. The broad spectral feature near 1.085 μm is unidentified. In the first positive system, the (4,5) band of $N_2(B^3\Pi_g)$ emits at 1.074 μm and, thus, overlaps with the (0,0) of NCl($a^1\Delta$) at 1.077 μm. If the (4,5) band were present, other nearby transitions such as the (2,3) (λ = 1.14 μm) and (3,4) (λ =1.11 μm) bands may also be evident. Spectral scans were made in this region, but the presence of the (2,3) and (3,4) bands was not observed. However, we note the Franck−Condon factors[16] for these transitions are much weaker than the (4,5) band (the 3,4 band is a factor of 10 less than the 4,5 band), and thus, their emission may be so diminished that they lie below the detection limit of the system. Whether the fast decay component is nitrogen first positive or some other unidentified process, we treat it as an independent first-order decay. In this regard, the kinetic model described by eq 9 was modified by adding to it an independent first-order decay of the form $I'(t) = I'(t)_0 \exp(-k_1 t)$:

$$I(t) = \frac{k'_1[\mathrm{NCl(a)}]_0}{\exp(k'_1 t)(k_2[\mathrm{NCl(a)}]_0 + k'_1) - k_2[\mathrm{NCl(a)}]_0} + I'(t)_0 \exp(-k_1 t) \quad (10)$$

where $I'(t)_0$ is initial intensity of the fast decay component and k_1 is the first-order rate constant.

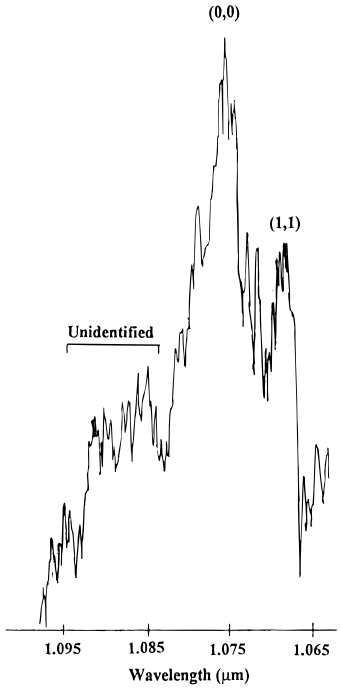

Figure 7. Spectrum of the near-infrared emission produced from the 193 nm photolysis of ClN_3. The (0,0) and (1,1) bands of the NCl($a^1\Delta - X^3\Sigma^-$) transition are identified. An unidentified spectral feature near 1.085 μm is observed.

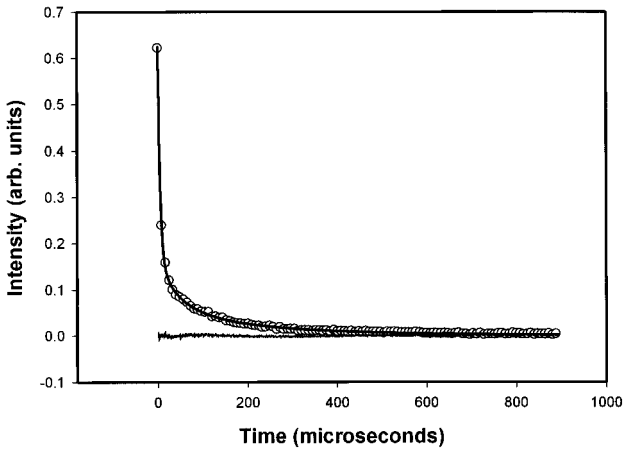

Figure 8. Nonlinear least-squares fit (solid line) of the sum of an independent first-order and second-order decay described by eq 10 to the observed NCl(a) decay (○) in Figure 4a. The lower trace is the residual analysis of the least-squares fit. A value of $(7.5 \pm 0.9) \times 10^{-12}$ cm^3/(molecule s) for the NCl(a) bimolecular self-annihilation rate constant and $(5.7 \pm 1.4) \times 10^{-13}$ cm^3/(molecule s) for the ClN_3 quenching rate constant are obtained. The independent first-order rate constant is 2.0×10^5 s^{-1}.

Figure 8 shows a nonlinear least-squares fit of the independent first- and second-order decay model to the NCl($a^1\Delta$) time decay in Figure 4a. Shown with Figure 8 is the residual analysis and suggests the model accurately accounts for both the independent first-order and second-order NCl($a^1\Delta$) decays. Accordingly, a

TABLE 2: Summary of the Parameter Contribution for the NCl($a^1\Delta$) Decay Model

parameter	rel % of obsd decay[a]
$[NCl(a^1\Delta)]_0$	56.2
k'_1	6.0
k_2	35.5
$I_0'(t)$	0.3
k_1	2.0

[a] These values are obtained by calculating the range of the minimum and maximum partial derivatives of a parameter, multiplying the range by the fitted parameter value, and normalizing to 100%.

value of (7.5 ± 0.9) (2σ) × 10^{-12} cm^3/(molecule s) is obtained for the NCl($a^1\Delta$) self-annihilation rate constant, (5.7 ± 1.4) × 10^{-13} cm^3/(molecule s) for the ClN_3 quenching rate and 2.0 × 10^5 s^{-1} for the fast first-order decay component, k_1. The uncertainty in each rate constant (k_2 and k'_1) arises from the accumulated uncertainties from the titration (see Appendix), the residual ClN_3 density, and the confidence intervals from the least-squares fit. The largest source of error for the residual ClN_3 density stems from the measuring the fluence (in particular, the beam area, ±25%). The coefficient of determination r^2 for the data shown in Figure 8 is 0.998. However, eq 10 is a five-parameter fit to the observed NCl($a^1\Delta$) decay. Because of the large number of adjustable parameters, r^2 is not necessarily the best figure of merit for the kinetic model. A sensitivity analysis of the parameters in eq 10 across the intensity−time domain in Figure 8 is perhaps a better test of model accuracy. Table 2 is a summary of the parameter influence across the entire NCl($a^1\Delta$) decay. The values are expressed as a relative percentage of the entire NCl($a^1\Delta$) decay and illustrate the magnitude a particular parameter has on the overall time decay. Each parameter contributes significantly to the overall decay, suggesting the model adequately describes the loss of NCl($a^1\Delta$) in the system. Several bimolecular rate constant determinations were performed with the results summarized in Table 1. The average NCl($a^1\Delta$) self-annihilation rate constant is (7.2 ± 0.9) × 10^{-12} cm^3/(molecule s). The NCl($a^1\Delta$) bimolecular self-removal rate was first addressed by Benard and co-workers[17] in a study of the thermal decomposition of ClN_3 into NCl($a^1\Delta$). A value of 8 × 10^{-12} cm^3/(molecule s) for the self-annihilation rate constant was obtained by calculating the yield of NCl($a^1\Delta$) from emission intensities and known Einstein A coefficients. Due to the uncertainty in A, the rate constant is an approximate value; however, it is not inconsistent with the rate constant reported here. The magnitude of the NCl($a^1\Delta$) self-annihilation rate is also comparable the analogous NF($a^1\Delta$) self-removal rate constant of (5 ± 2 × 10^{-12} cm^3/(molecule s) reported by Du and Setser.[18]

The NCl($a^1\Delta$) bimolecular self-removal rate in reaction 4 describes a process in which the NCl($a^1\Delta$) radicals are removed via chemical reaction. The "products" of the self-quenching process are many, and numerous energetically available products are possible including 2Cl + $N_2(v)$, NCl_2 + N, and 2NCl(X). The energy pooling reaction, 2NCl($a^1\Delta$) → NCl($b^1\Sigma^+$) + NCl($X^3\Sigma^-$), is another possible channel for NCl($a^1\Delta$) self-removal. No attempt was made to quantify the pooling process; however, the analogous NF($a^1\Delta$) pooling reaction is a minor component of the total self-annihilation reaction,[18] and most of the self-removal of NCl($a^1\Delta$) is probably due to chemical processes. Although reaction 5 is treated as a simple quenching process, NCl($a^1\Delta$) + ClN_3 → NCl($X^3\Sigma^-$) + ClN_3, other chemical processes can be drawn for five in which $N_2(v)$ or NCl($a^1\Delta$) is regenerated, for example, NCl($a^1\Delta$) + ClN_3 → NCl($a^1\Delta$) + NCl($X^3\Sigma^-$) + $N_2(v)$. However, the 193 nm photolysis results presented here are consistent with a kinetic model in which NCl($a^1\Delta$) radicals decay by simple homogeneous and mixed bimolecular reaction pathways.

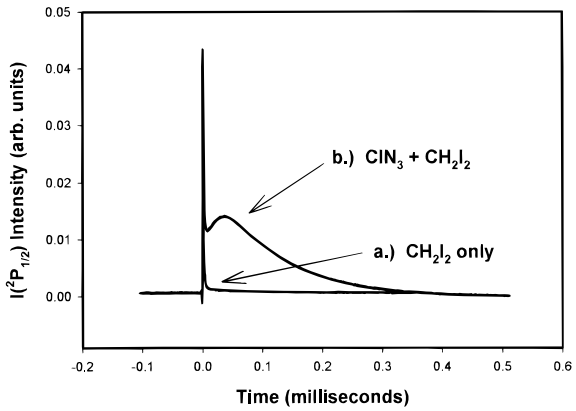

Figure 9. (a) Time profile of the I($^2P_{1/2}$−$^2P_{3/2}$) emission from the 193 nm photolysis of only CH_2I_2. Photolysis conditions: laser fluence = 210 mJ/cm^2, CH_2I_2 density = 2.2 × 10^{14} molecules/cm^3. (b) Time profile of the I($^2P_{1/2}$−$^2P_{3/2}$) emission from the 193 nm photolysis of a mixture of CH_2I_2 and ClN_3. Photolysis conditions: laser fluence = 210 mJ/cm^2, CH_2I_2 density = 2.2 × 10^{14} molecules/cm^3, ClN_3 density = 7.8 × 10^{15} molecules/cm^3. The intense feature at short times in (a) and (b) is believed to be $I_2(B^3\Pi_u \rightarrow X^1\Sigma_{0g})$ emission. The I($^2P_{1/2}$−$^2P_{3/2}$) emission was isolated with an interference filter at 1.315 μm and observed with an intrinsic Ge detector (77 K).

Photolysis of CH_2I_2/ClN_3 Mixtures. The rate constant for the pumping of I($^2P_{1/2}$) by NCl($a^1\Delta$) is (1.8 ± 0.3) × 10^{-11} cm^3/(molecule s).[6] To assess the magnitude of the bimolecular self-removal rate constant measured here in relation to the I($^2P_{1/2}$) pumping rate by NCl($a^1\Delta$), a mixture of CH_2I_2 and ClN_3 was prepared and photolyzed at 193 nm. We note the branching fraction of ground state I($^2P_{3/2}$) from CH_2I_2 is ≥ 0.95 at the 193 nm photolysis wavelength.[19] Further, Ray and Coombe[8] have concluded that the secondary photolysis CH_2I is not a significant source of I($^2P_{1/2}$) emission at 193 nm. Figure 9a shows the I($^2P_{1/2}$) emission time profile resulting from the photolysis 193 nm of only CH_2I_2 at a density of 2.2 × 10^{14} molecules/cm^3 and a laser fluence of 210 mJ/cm^2. The rapid and intense spike in Figure 9a at short times (within the 15 μs detector time constant) arises from CH_2I_2 photolysis and is identified as $I_2(B^3\Pi_u \rightarrow X^1\Sigma_{0g})$ emission.[19] Figure 9b shows the I($^2P_{1/2}$) emission time profile under the same photolysis conditions but with the addition of 5.7 × 10^{15} molecules/cm^3 of ClN_3. The time profile shows a prompt $I_2(B^3\Pi_u)$ spike followed by a rise and a slow decay of significantly enhanced I($^2P_{1/2}$) emission over several hundred microseconds due to the collisional pumping by NCl($a^1\Delta$). A nearly 3-fold increase in the I($^2P_{1/2}$) emission intensity over that of just CH_2I_2 photolysis is observed. Clearly, despite the relatively rapid NCl($a^1\Delta$)−NCl($a^1\Delta$) self-annihilation rate, the I($^2P_{1/2}$) pumping by NCl($a^1\Delta$) remains a dominant process.

Summary and Conclusions

The second-order decay kinetics of NCl($a^1\Delta$) resulting from the pulsed 193 nm photolysis of ClN_3 was studied, and a gas phase transient titration scheme calibrated the absolute NCl($a^1\Delta$) densities. Using these absolute NCl($a^1\Delta$) densities and a kinetic model that accounts for the second-order time behavior of NCl($a^1\Delta$), the bimolecular self-annihilation rate constant of NCl($a^1\Delta$) is found to be 7.2 ± 0.9 × 10^{-12} cm^3/(molecule s). Despite the rapid self-removal rate, intense I($^2P_{1/2}$) emission is still observed when mixtures of CH_2I_2 and ClN_3 are photolyzed at 193 nm. The significant NCl($a^1\Delta$) bimolecular rate constant suggests the transport of this metastable in chemical laser

systems must be short unlike the COIL system where the $O_2(a^1\Delta)$ bimolecular rate[9] is slow, $k = 5 \times 10^{-17}$ cm^3/(molecule s), and facilitates long transport times and efficient extraction of the metastable energy. Thus, an $NCl(a^1\Delta)$-based system would necessitate a short mixing region to overcome $NCl(a^1\Delta)$ self-annihilation losses. Future work will be directed at measuring the effects of high temperature on the self-annihilation process, the $NCl(a^1\Delta) + I(^2P_{3/2})$ energy transfer reaction, and the quenching of $NCl(a^1\Delta)$.

Acknowledgment. This work is supported by the Air Force Office of Scientific Research.

Appendix

$NCl(a^1\Delta)$ Titration. Second-order rate coefficients require knowledge of the absolute concentration of the reactants. In photolytic studies as those presented here, the absolute densities are typically obtained by a transient absorption measurement. However, the $NCl(a^1\Delta - X^3\Sigma^-)_{v=0}$ transition occurs at 1.08 μm and makes the absorption measurement difficult. In this respect, a gas phase quenching titration was developed to measure absolute $NCl(a^1\Delta)$ density. The method involves photolyzing ClN_3 to produce $NCl(a^1\Delta)$:

$$ClN_3 + h\nu\ (193\ \text{nm}) \rightarrow NCl(a^1\Delta) + N_2 \quad \text{(A.1)}$$

$$\rightarrow NCl(b^1\Sigma^+) + N_2$$

$$\rightarrow NCl(X^3\Sigma^-) + N_2(A^3\Sigma^+_u)$$

The $NCl(a^1\Delta)$ fluorescence is quenched or titrated by the addition of a known amount of quencher, Q_2:

$$NCl(a^1\Delta) \rightarrow NCl(X^3\Sigma^-) + h\nu\ (1.08\ \mu\text{m}) \quad \text{(A.2)}$$

$$NCl(a^1\Delta) + Q_2 \rightarrow NClQ + Q \quad \text{(A.3)}$$

The NCl(a) intensity is then monitored at various reaction times after the laser pulse. However, due to the presence of the fast decay component ($k \simeq 2 \times 10^5$ s^{-1}), the titration data were not collected until at least 15 μs of reaction time had transpired. The amount of added quencher to titrate the $NCl(a^1\Delta)$ intensity to zero is taken as the initial $NCl(a^1\Delta)$ concentration in the system. A scaling factor (in units of V cm^3/molecule) is derived from the ratio of the peak fluorescent $NCl(a^1\Delta)$ amplitude (in V) to the titrated $NCl(a^1\Delta)$ density (molecules/cm^3) and converts the observed $NCl(a^1\Delta)$ amplitude to a number density. To determine the second-order rate constant k_2, a nonlinear least-squares fit of an $NCl(a^1\Delta)$ kinetic model to an $NCl(a^1\Delta)$ time profile is performed. The rate constant is extracted (in V^{-1} s^{-1}) and is converted to a second−order rate constant by applying the scaling factor. The ClN_3 quenching rate constant, k'_2, is obtained by dividing the fitted value of k'_1 (in units of s^{-1}) by the residual ClN_3 density. The accuracy of titration is contingent on accurate measurements of the titrant density (the mass flow uncertainty is ±5%) and the absence of secondary chemistry since competing reactions between the added titrant and the $N_2(A^3\Sigma^+_u)$, $NCl(b^1\Sigma^+)$, and $NCl(X^3\Sigma^-)$ photoproducts would skew the titration to higher end point values. However, the photolysis yields[11,20] of these species are small (≤1%), and any secondary reactions with the titrant are not expected to occur.

Several requirements must be met for a successful titration. First, reaction A.3 must proceed chemically so that the amount of titrant consumed can be directly related to $NCl(a^1\Delta)$ density. Previous mass spectroscopic studies by Clyne et al.[22] on the $NCl(a^1\Delta) + Cl_2$ reaction demonstrate the rapid production of NCl_2 and Cl, whereas the reaction between ground state $NCl(X^3\Sigma)$ and Cl_2 is unreactive. More recent studies by Du and Setser[23] and Ray and Coombe[12] have focused on the mechanisms of the $NCl(a^1\Delta) + Cl_2$ and $NF(a^1\Delta) + Br_2$ reactions. They have shown these reactions to proceed chemically through an insertion step (established through correlations of measured rate constants and ionization potentials) to form a vibrationally excited amine-like intermediate followed by dissociation:

$$NCl(a^1\Delta) + Cl_2 \rightarrow NCl_3^* \rightarrow NCl_2 + Cl \quad \text{(A.4a)}$$

$$\rightarrow NCl(X) + Cl_2 \quad \text{(A.4b)}$$

$$NF(a^1\Delta) + Br_2 \rightarrow NFBr_2^* \rightarrow NFBr + Br \quad \text{(A.5a)}$$

$$\rightarrow NBr(X) + BrF \quad \text{(A.5b)}$$

$$\rightarrow NF(X) + Br_2 \quad \text{(A.5c)}$$

Indeed, no evidence for physical E to V quenching[12,23] is seen in the quenching of $NCl(a^1\Delta)$ by Cl_2 and $NF(a^1\Delta)$ by Cl_2 and Br_2. Since the product analyses of reactions A.4 and A.5 suggest the dominant pathways are channels A.4a and A.5a,[22,23] it is reasonable to presume the analogous chemical reaction occurs between Br_2 and $NCl(a^1\Delta)$:

$$NCl(a^1\Delta) + Br_2 \rightarrow NClBr_2^* \rightarrow NClBr + Br \quad \text{(A.6)}$$

In light of Figure 4, it appears that some of the $NCl(a^1\Delta)$ is removed by secondary reactions. As such, the titrant quenching rate constant must also be very large (that is, a reaction on nearly every collision) with respect to all other loss channels. This ensures that eq A.3 is completed at any reaction time and essentially all the $NCl(a^1\Delta)$ is removed through the $Q_2 + NCl(a^1\Delta)$ reaction channel.

To more fully understand and gauge the utility the titration experiment, measurements were undertaken to obtain the F_2, Cl_2, and Br_2, quenching rate constants for $NCl(a^1\Delta)$. These experiments were performed by recording the time history of $NCl(a^1\Delta)$ resulting from the 193 nm photolysis of ClN_3/quencher mixtures. We note the photodissociation of these species at 193 nm is expected to be small since the absorption cross sections[21] are about 10^{-20} cm^2. The ClN_3 density was held at a constant value, and variable amounts of quencher gas were added in a large, 4−10-fold excess over the $NCl(a^1\Delta)$ density to maintain pseudo-first-order kinetics. Care was taken to minimize the effects of the $NCl(a^1\Delta)-NCl(a^1\Delta)$ bimolecular rate by reducing the laser fluence to 65 mJ/cm^2 and the ClN_3 density to less than 1.5×10^{15} molecules/cm^3. Figure 10a shows a time history of $NCl(a^1\Delta)$, indicating the presence of a fast decay element of a few μs followed by a slow decay component of several tens of microseconds. In accordance with the previous observation of a fast independent first-order process, the decay curves were fit to a sum of two independent first-order decays, $I(t) = I'_0 \exp(-t/\tau') + I_0 \exp(-t/\tau)$, where $1/\tau'$ and $1/\tau$ are the rates for the rapid and slow decay components, respectively. The $NCl(a^1\Delta)$ quenching rates, k (s^{-1}), were obtained from a least-squares fit of the slow decay component and are plotted as a function of quencher density Q_2 (molecules/cm^3), $\lambda = k_q[Q_2] + k_0$, where k_0 is comprised of contributions from quenching by Cl_2 and ClN_3 and the radiative decay of $NCl(a^1\Delta)$. Since the radiative rate of $NCl(a^1\Delta)$ is small,[15] its contribution to the decay is negligible, and decay rates at $[Q_2] = 0$ are largely due to residual ClN_3 and any background Cl_2

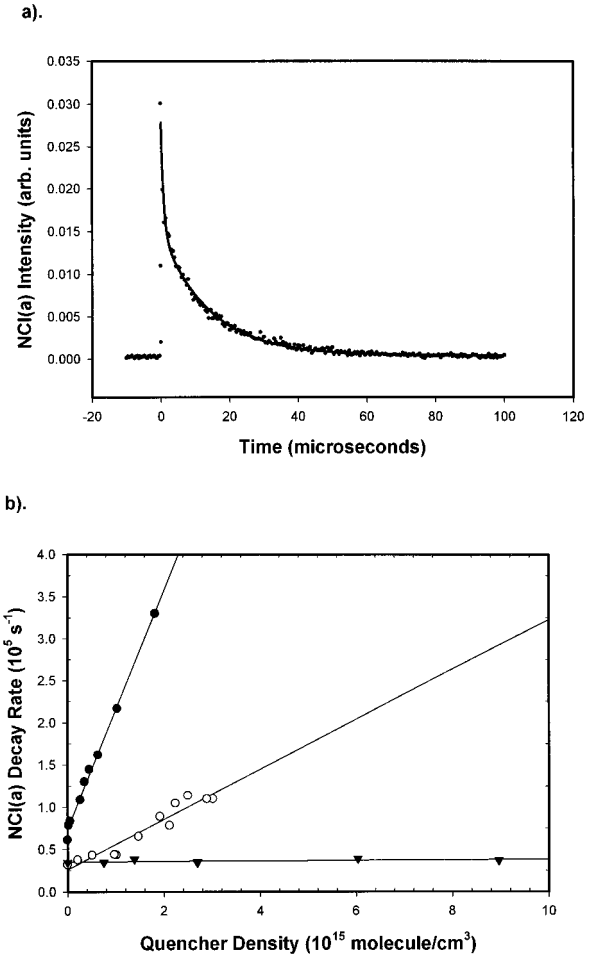

Figure 10. (a) A least-squares fit of two first-order independent decays of the form $I = I'_0 \exp(-t/\tau') + I_0 \exp(-t/\tau)$ to an NCl(a−X)$_{v=0}$ time decay where $1/\tau'$ and $1/\tau$ are the rates for the rapid and slow decay components, respectively. Photolysis conditions: laser fluence = 65 mJ/cm^2, initial ClN_3 density = 1.6×10^{15} molecules/cm^3, total pressure = 2.3 Torr. (b) Stern−Volmer plots quenching of NCl(a) by (●) Br_2, (○) Cl_2, and (▼) F_2 for the slow component. The solid lines drawn represent a least-squares fit to the slow decay data.

TABLE 3: Quenching Rate Constants for NCl($a^1\Delta$) and NF($a^1\Delta$) in 10^{-13} cm^3 molecule^{-1} s^{-1}

halogen	NCl($a^1\Delta$)[a]	NCl($a^1\Delta$)[b]	NF($a^1\Delta$)[c]
F_2	2.5 ± 1.1		0.32 ± 0.03
Cl_2	290 ± 60	180 ± 30	5.8 ± 0.6
Br_2	1400 ± 200		380 ± 60
I_2			1500 ± 200

[a] Values obtained in this work. [b] Reference 12. [c] Reference 23.

quenching. Stern−Volmer treatment of the slow decay component for the collisional quenching of the $\Delta v = 0$ band of NCl($a^1\Delta$) at 1.08 μm by F_2, Cl_2,and Br_2 is shown in Figure 10b. The rate constants are determined from a least-squares fit to the data as indicated by the solid lines. These values are summarized in Table 3 along with a comparison of the quenching of isovalent NF($a^1\Delta$) by these species. The value for Br_2 is (1.4 ± 0.2) (2σ) × 10^{-10} cm^3/s and suggests that Br_2 is a very rapid quencher of NCl($a^1\Delta$). Quenching by Cl_2 is (2.9 ± 0.6) (2σ) × 10^{-11} cm^3/(molecule s) is also rapid. However, only the magnitude of the Br_2 rate constant can provide the necessary quenching characteristics in view of the secondary loss channels of NCl($a^1\Delta$) in this system.

Figure 11a shows a consistency check for the Br_2 titration at two reaction times of 15 and 100 μs. A third titration at a reaction time of 200 μs was also performed but is omitted for

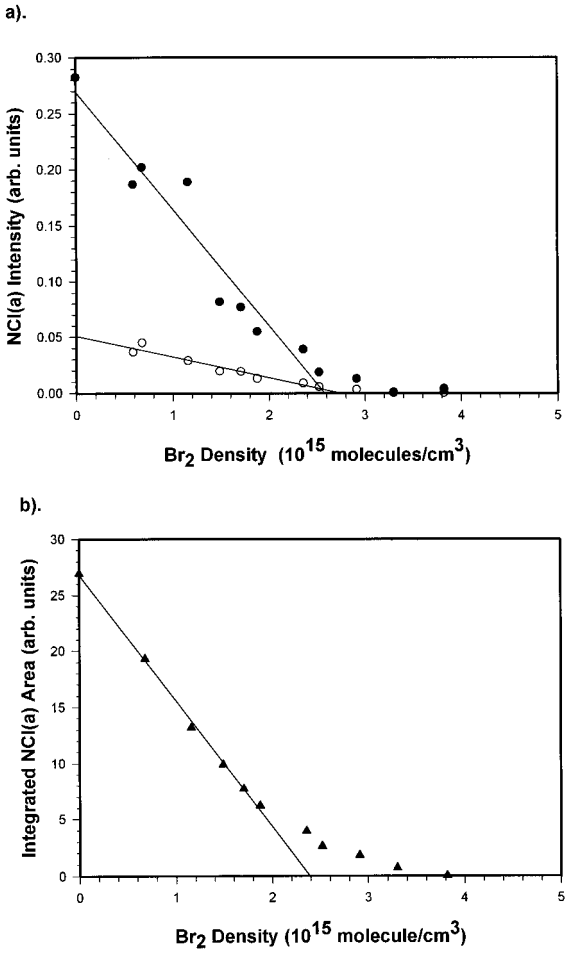

Figure 11. Comparison of a Br_2 titration for the initial NCl(a) density using fixed reaction time and time-integrated intensity methods resulting from the ArF photodissociation of ClN_3. Photolysis conditions: laser fluence = 67 mJ/cm^2, ClN_3 density = 7.4×10^{15} molecules/cm^3, total pressure = 4.6 Torr. The end point is obtained by extrapolation off the linear portion of the titration plot to the Br_2 axis. (a) Fixed reaction times: (●) = 15 μs, (○) = 100 μs. An average titrated initial NCl(a) density of (2.4 ± 0.8) × 10^{15} molecules/cm^3 is obtained. (b) Time-integrated intensities. A titrated initial NCl(a) density of (2.4 ± 0.2) × 10^{15} molecules/cm^3 is obtained.

clarity. The titration is collected at an initial ClN_3 density of 7.4×10^{15} molecules/cm^3, a laser fluence of 67 mJ/cm^2, and a total pressure of 4.7 Torr. The end points are obtained by extrapolation off the linear portion of the titration plot to the Br_2 axis. Accordingly, the initial NCl($a^1\Delta$) density for the 15, 100, and 200 μs reaction times yields equal end points (±15%) of 2.6×10^{15}, 2.7×10^{15}, and 1.9×10^{15} molecules/cm^3, respectively, and thus Br_2 is deemed a valid titrant. However, we find the intensity data too weak and noisy at reaction times greater than 300 μs for an accurate extrapolation. To avoid this limitation, an alternative approach to titrating the initial NCl($a^1\Delta$) density is made by fully time integrating the NCl($a^1\Delta$) intensity profile as a function of added Br_2 density. The NCl($a^1\Delta$) density, N, is proportional to the intensity of NCl($a^1\Delta$), I_{NCl}, and its A coefficient, $I_{NCl} \propto NA$ or $I_{NCl}\tau \propto N$. The product $I_{NCl}\tau$ gives is the integrated NCl($a^1\Delta$) density. As a quencher is added, the product of the lifetime and the intensity ($I_{NCl}\tau$) is reduced in proportion to NCl($a^1\Delta$) density. Figure 11b illustrates the experimental time integrated titration with an end point of (2.4 ± 0.4) × 10^{15} molecules/cm^3 and compares favorably to the fixed point titrations of 15, 100, and 200 μs in Figure 11a. In determining the bimolecular self-annihilation rate constants above, we adopted the time-integrated intensity method for measuring the initial NCl($a^1\Delta$) density.

References and Notes

(1) McDermott, W. E.; Pchelkin, N. R.; Benard, D. J.; Bousek, R. R. *Appl. Phys. Lett*. **1978**, *32*, 469.

(2) Benard, D. J.; McDermott, W. E.; Pchelkin, N. R.; Bousek, R. R. *Appl. Phys. Lett.* **1979**, *34*, 40.

(3) Perram, G. P. *Bibliography of Short Wavelength Chemical Laser Research*, 1993**,** AFIT/EN/TR/93-03, Department of Engineering Physics, Air Force Institute of Technology, Wright-Patterson AFB, OH 45433-7765.

(4) Benard, D. J. *J. Appl. Phys.* **1993**, *74*, 2900.

(5) Bower, R. D.; Yang, T. T. *J. Opt. Soc. Am. B* **1991**, *8*, 1583.

(6) Ray, A. J.; Coombe, R. D. *J. Phys. Chem.* **1993**, *97*, 3457.

(7) Yang, T. T.; Gylys, V. T.; Bower, R. D.; Rubin, L. F. *Opt. Lett.* **1992**, *24*, 1803.

(8) Ray, A. J.; Coombe, R. D. *J. Phys. Chem.* **1995**, *99*, 7849.

(9) Lilenfeld, H. V. *Oxygen-Iodine Laser Kinetics*, 1983, AFWL-TR-83-01, Phillips Laboratory (formerly Air Force Weapons Laboratory), Kirtland Air Force Base, NM 87117.

(10) Fujii, H.; Atsuta, T.; Masuda, W. *Proceedings of the Fourth International Workshop on Iodine Lasers and Applications*; *SPIE* **1995**, *2767*, 170.

(11) Coombe, R. D.; Patel, D.; Pritt, A. T., Jr.; Wodararczyk, F. J. *J. Phys. Chem.* **1981**, *75*, 2177.

(12) Ray, A. J.; Coombe, R. D. *J. Phys. Chem*. **1994**, *98*, 8940.

(13) (a) Zuev, V. S., Mikheev, L. D. in *Photochemical Lasers*; Harwood Academic Publishers: Langhorne, PA, 1991; p 29. (b) Krupke, W. F.; George, E. V.; Haas, R. A. In *Laser Handbook*; Stich, M. L., Ed., North-Holland Publishing: New York, 1979; Vol. 3, p 698. The profile for the residual ClN_3 density at a distance z into the medium and time t is described by the following equation: $N_z(z,t) = N_0\{1 + \exp[(V_b t - z)\sigma_{193}N_0] - \exp[-z\sigma_{193}N_0]\}^{-1}$ where σ_{193} is the absorption cross section of ClN_3 at 193 nm, 2.6×10^{-18} cm^2, and N_0 is the initial ClN_3 density. V_b is the bleaching wave velocity, $V_b = [I_0/h\nu]/[N_0 + I_0/ch\nu]$, where $I_0/h\nu$ is the photon fluence rate ($h\nu$/cm^2 s), $I_0/ch\nu$ is the photon density ($h\nu$/cm^3), and c is the speed of light.

(14) (a) Arunan, E.; Liu, C. P.; Setser, D. W.; Gilbert, J. V.; Coombe, R. D. *J. Phys. Chem.* **1994**, *98*, 494. (b) Clark, T. C.; Clyne, M. A. A. *Trans. Faraday Soc*. **1970**, *66*, 877. The exothermicity for the photodissociation $ClN_3 + h\nu$ (248 nm) $\rightarrow$ NCl(a) + N_2(X) is 108 kcal/mol based on a ΔH^0_f(NCl(a)) = 100.5 kcal/mol in (a) and a $\Delta H^0_f(ClN_3)$ = 93 kcal/mol in (b).

(15) (a) Yarkony, D., Jr. *Chem. Phys.* **1987**, *86*, 1642. (b) Becker, A. C.; Schurath, U. *Chem. Phys. Lett.* **1989**, *160*, 586.

(16) Lofthus, A.; Krupenie, P. H. *J. Phys. Chem. Ref. Data* **1977**, *6*, 263.

(17) Benard, D. J.; Chowdhury, M. A.; Winker, B. K.; Seder, T. A.; Michels, H. H. *J. Phys. Chem.* **1990**, *94*, 7507.

(18) Du, K.; Setser, D. W. *J. Phys. Chem.* **1990**, *94*, 2425.

(19) Pence, W. H.; Baughcum, S. L.; Leone, S. R *J. Phys. Chem*. **1981**, *85*, 3844.

(20) Coombe, R. D.; David, S. J.; Henshaw, T. L.; May, D. J. *Chem. Phys. Lett.* **1985**, *120*, 433.

(21) Unpublished results. The absorption cross section for Br_2 and Cl_2 at 193 nm are 3×10^{-20} and 1×10^{-20} cm^2, respectively.

(22) (a) Clyne, M. A. A.; MacRobert, A. J. *J. Chem. Soc., Faraday Trans. 2* **1983**, *79*, 283. (b) Clyne, M. A. A.; MacRobert, A. J.; Brunning, J.; Cheah, C. T. *J. Chem. Soc., Faraday Trans. 2* **1983**, *79*, 1515.

(23) Du, K.; Setser, D. W. *J. Phys. Chem.* **1992**, *96*, 2553.